DOI: 10.2352/ISSN.2470-1173.2016.18.DPMI-007

Method for Quantifying Image Sensor Susceptibility to Chromatic Flare Artifacts

Orit Skorka, Dave Jasinski, Radu Ispasoiu, and Vladi Korobov
Image Sensor Group, ON Semiconductor, San Jose, CA, USA

Abstract

Chromatic flare artifacts, purple flare in particular, are objectionable color artifacts affecting image quality in digital photography systems ranging from DSLR to mobile imaging cameras. Although they originate from internal reflections and scattering in the camera module, they can be diminished with proper pixel design strategies. This work presents a method to quantify an image sensor susceptibility to chromatic flare artifacts. It is based on measurements of the spectral response of pixels for varied angles of incidence, and subsequent analysis of color properties of synthetic images that are processed through a conventional pipeline. Experimental work has been done with image sensors that differ by their color filter array and grid properties. Results show that use of metal grid and deep trench isolation—state-of-the-art pixel fabrication approaches that were developed to suppress crosstalk—are advantageous for mitigation of chromatic flare artifacts.

Introduction

Chromatic flare artifacts can appear in digital images due to light rays that enter the silicon substrate at high angles of incidence. At camera level, this can be caused by various factors, including internal reflections, volume scattering, scattering at the aperture edge, and scattering due to lens roughness and dirt particles in the module. The resulting high angles of light incidence may lead to absorption of photons by photodiodes (PDs) that neighbor the desired one. **Figure 1** presents the chromatic (purple) flare artifact in an image that was captured with an iPhone5C camera.

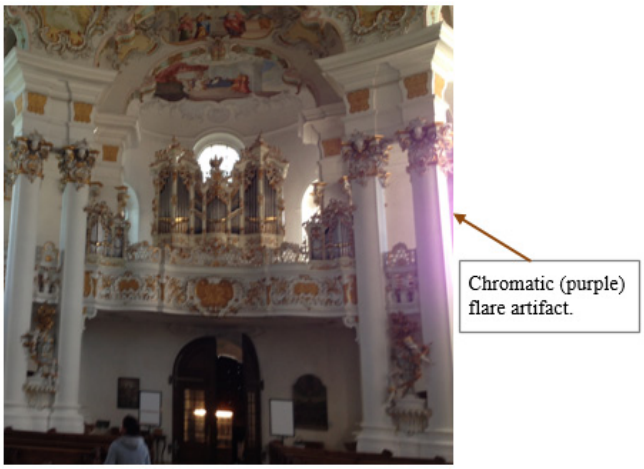

Figure 1 - Example photo that shows chromatic (purple) flare artifact in an image that was captured with an iPhone5C camera.

Camera module design strategies can be utilized to mitigate chromatic flare artifacts by reducing internal reflections. Chen [1], for example, presented a method for optimization of the camera lens for mobile phone applications to reduce internal reflections at the cost of degraded modulation transfer function. Aperture design can also be optimized to reduce internal reflections by blocking light rays at high angles from entering the camera module, but this may cut image plane illuminance. A different approach is to apply pixel design strategies that prevent light rays at high angles of incidence from entering the substrate.

At present, there are commercially available methods for characterization of veiling glare, which is a non-chromatic flare artifact that adds black level offset [2], [3]. However, to our knowledge, there are no customary methods for characterization of chromatic flare artifacts. This work proposes a method to quantify an image sensor susceptibility to those artifacts, and presents evaluation results from experimental work with several pixel structures.

How Do Chromatic Flare Artifacts Develop?

Both hardware and software of a digital camera contribute to appearance of chromatic flare artifacts in a processed image. Those artifacts are initiated by optical crosstalk and then amplified by the processing pipeline for color-imaging.

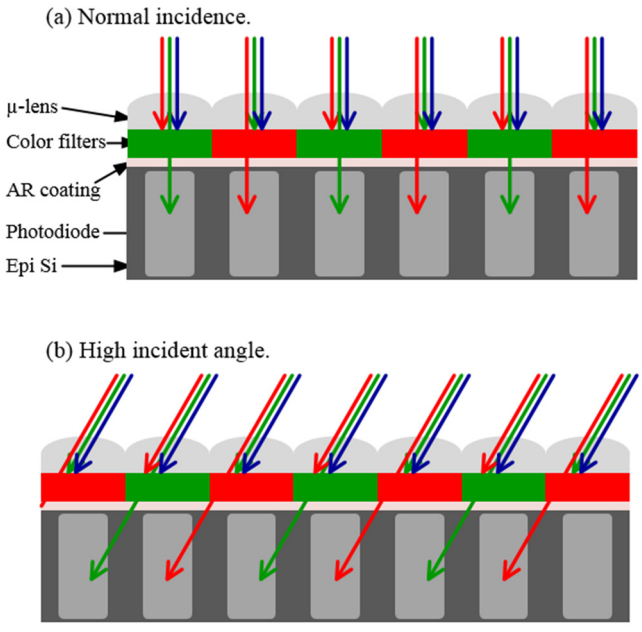

Figure 2 – (a) In normal incidence, photons are filtered by the color filter before reaching the photodiode. (b) In high angles of incidence, some photons may be filtered by the color filter of a certain pixel but reach a photodiode of a neighboring one.

DOI: 10.2352/ISSN.2470-1173.2016.18.DPMI-007

Optical Crosstalk

These days, the traditional RGGB Bayer color filter array (CFA) pattern is commonly used in digital cameras for consumer use applications.

Figure 2 shows an illustration of the absorption of light rays at normal and high angles of incidence. The figure refers to the R-G row of a RGGB CFA, but the situation in the G-B row is similar. In normal incidence, if optical crosstalk due to reflections in the silicon substrate is excluded, all photons that reach the pixel PD must first pass through its color filter, as shown in **Figure 2** (a). With light rays that arrive at high angles of incidence, photons enter the μ-lens and color filter array in directions that allow some of them to reach and be absorbed by PDs of neighboring pixels, as shown in **Figure 2** (b), and this causes optical crosstalk.

The Color-Imaging Pipeline

The amount of charge that is accumulated in each pixel is converted to voltage and, then, to a digital signal. In the raw (Bayer) image, each pixel includes digital data of a single color. Conventional processing pipelines for color imaging are composed of processing blocks that perform demosaic, white-balance, color correction, and gamma correction [4]. Each pixel in the (processed) output image stores the digital level of the R, G, and B colors. White-balance (WB) and color correction matrix (CCM) coefficients are determined from the sensor response to normal incidence light. **Figure 3** shows a simplified diagram of the color-imaging pipeline.

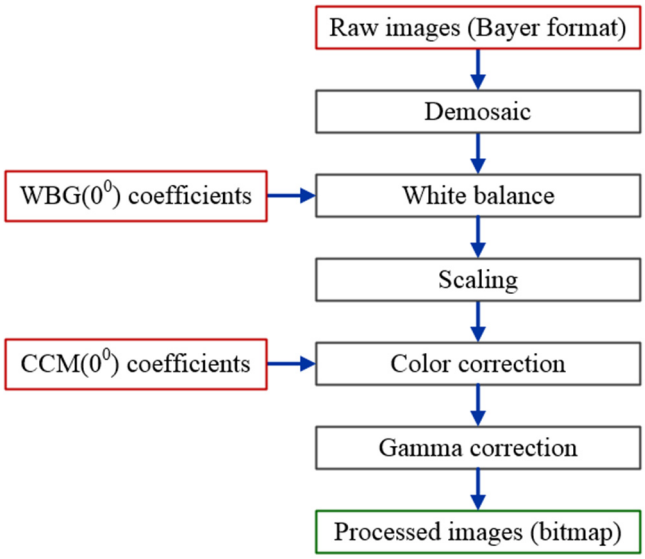

Figure 3 – Processing blocks in a conventional color-imaging pipeline.

With RGGB CFAs, chromatic artifacts usually appear purple because transparency of G color filters is somewhat higher than that of R and B ones. Therefore, more high-angle rays are able to pass through the G filter and be absorbed in PDs of R and B neighboring pixels than vice versa. In addition, sensitivity of R and B pixels to broadband white illuminants is typically lower than that of G pixels, partially, due to lower R and B filter transparency. Therefore, digital gain is applied to their signals by the processing pipeline at the white balance stage, and this further amplifies the error that was originated by the optical crosstalk. When R/G and B/G signal ratios are higher than expected from the normal incidence response, the end result is enhanced purple in the final image.

Proposed Method

As the goal of this work is to isolate the sensor and characterize its own susceptibility to chromatic flare artifacts, the method here cannot rely on image capture, where a complete camera module is needed; instead, it must use the sensor properties in order to draw conclusions. The method requires characterization of the spectral response of all color pixels at varied angles of incidence. Measurement results are used to simulate synthetic raw images, which are processed through a conventional color pipeline. The sensor susceptibility to chromatic flare artifacts is derived by analyzing the color properties of the processed images.

Sensor Quantum Efficiency

Quantum efficiency (QE) represents the ratio between the number of electrons that are generated in the photodiode and the number of incident photons. Description of a setup and methodology for QE measurement can be found in [5]. To characterize the sensor optical crosstalk when light rays at high angles of incidence, in addition to normal incidence, the sensor QE is also characterized for higher angles of incidence. **Figure 4** presents a simplified diagram of the setup.

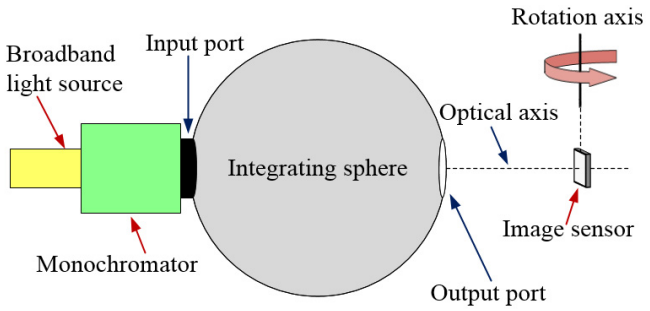

Figure 4 – Simplified diagram of a setup to characterize spectral response of an image sensor at different angles of incidence. The setup also includes a calibrated reference silicon PD (not shown), which is needed to derive QE.

When light rays that reach the image plane at high angles of incidence are absorbed by different photodiodes than desired, the shapes of the sensor QE curves that were produced from normal incidence measurement are not preserved. Changes in shapes of QE curves with incidence angle can indicate the amount of increase in optical crosstalk, but are insufficient to quantify the sensor susceptibility to chromatic flare artifacts.

Synthetic Images

QE curves that were measured at several angles of incidence are used to prepare synthetic raw images (by simulation) of light that is reflected from a uniform neutral color (gray) patch. A neutral color patch was chosen because it has no color (its chroma is 0, as later explained) and, therefore, any hue component that is found in the synthetic image indicates improper color reproduction. To generate synthetic images, the signal of each

DOI: 10.2352/ISSN.2470-1173.2016.18.DPMI-007

pixel in charge units, S_p, is calculated for an illuminant with a given spectral power distribution, I, expressed in W/(cm^2·µm) units, and a constant illuminance level. To simulate the response of a camera module, I is multiplied by transmission curves of a lens, T_{lens}, and an infra-red cut filter (IRCF), T_{IRCF}, as follows:

$$S_p = T_{int} A_p \int_{\lambda_1}^{\lambda_2} \frac{hc}{\lambda} \cdot I(\lambda) \cdot T_{lens}(\lambda) \cdot T_{IRCF}(\lambda) \cdot QE(\lambda) d\lambda, \quad (1)$$

where T_{int} is the integration time, which is constant for all cases, A_p is the pixel area, h is Planck constant, and c is the speed of light in vacuum. The term hc/λ is used in order to express $I(\lambda)$ in units of photon density. Integration is done from λ_1 = 400 nm to λ_2 = 700 nm to cover the entire pass band of the IRCF. The WB(0^0) and CCM(0^0) coefficients are optimized for the normal incidence response of all color planes.

Noise is added and uniformly distributed across the synthetic image in order to create a more realistic appearance, where noise parameter values are taken from the sensor electrical characterization results. The following temporal and structural noise sources are considered: readout noise, dark-current shot-noise, photon shot-noise, analog-to-digital converter (ADC) quantization noise, dark-signal non-uniformity (DSNU), and photo-response non-uniformity (PRNU).

The pipeline that is used to process the synthetic raw images includes standard processing blocks, as shown in **Figure 3**, and a simple chroma de-noising block. The pipeline normalizes pixel data after the raw data is white balanced. Therefore, to account for the effect of significant reduction in the pixel sensitivity with increase in incidence angle, white and black patches were added to small sections in the raw image, and it is assumed that QE of pixels where light from the white and black patches is reflected on the image plane is the normal incidence QE.

Color Analysis

Color properties of the output bitmap images are analyzed in order to assess the sensor susceptibility to chromatic flare artifacts. The standard RGB (sRGB) data that is stored in the bitmap images is converted to the CIELAB color space. In the CIELAB coordinates, the L* axis represents brightness level, and its value ranges from 0 (black) to 100 (white). The a* axis represents the red-green opponent hues, and the b* axis represents the yellow-blue opponent hues [6]. This is described in **Figure 5** (a).

Chroma represents colorfulness. It is, basically, the radius of a point in the a*b* circle, as shown in **Figure 5** (b), and it is calculated as:

$$C^*_{ab} = \sqrt{(a^*)^2 + (b^*)^2}. \quad (2)$$

With the processed synthetic images, chroma is calculated for the central region of each patch (the white and black reference regions are excluded). Chroma of processed images of designs that are less susceptible to chromatic artifacts should remain low even at high incidence angle.

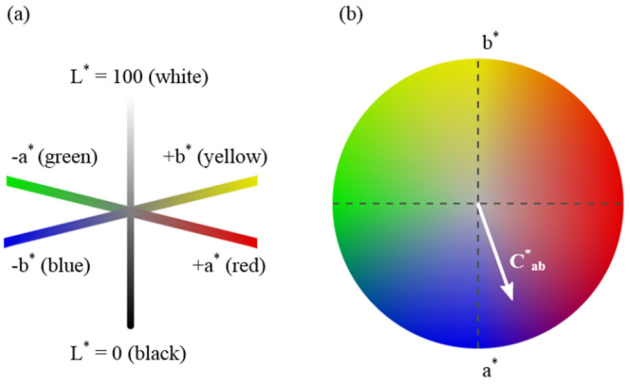

Figure 5 – (a) The CIELAB coordinates. L corresponds to brightness while a* and b* relate to the color components. (b) Chroma, C*ab, is the radius of a point in the a*b* circle. The central point, where C*ab = 0, has a neutral (gray) color. Code to generate this figure is based on a version by Westland et al. [7].*

Experimental Work

Four experimental back-side illuminated (BSI) image sensors were characterized for their susceptibility to chromatic flare artifacts. Pixel layout and peripheral circuitry of the four 1.1 µm BSI image sensors was similar, but they differed by properties of their color filter array and separation grid.

Test Structures

Figure 6 shows the CFA and separation grid of the four experimental test structures. In structure (a), a yellow color filter was used instead of a green one to form an RYYB CFA, and a dielectric wall (or a box when referring to the 3D structure) separates the color filters. Structure (b) is identical to structure (a), but with the commonly used RGGB CFA. The separation wall in structures (c) and (d) includes dielectric and metallic regions. Therefore, it is referred to as composite grid (CG). More configurations with metal-based grid are shown in [8].

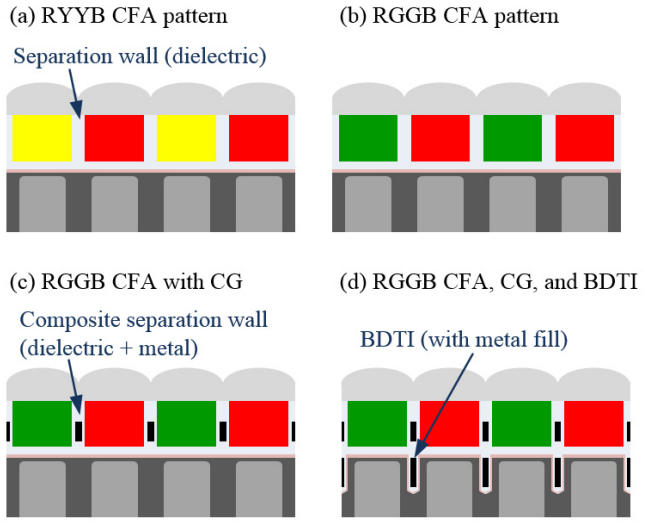

Figure 6 – Cross-section diagrams of the four test structures whose susceptibility to chromatic flare artifacts is characterized in this work. Structure (d) is the only one where modifications were applied to the silicon substrate, in the form of metal-filled backside isolation trenches

DOI: 10.2352/ISSN.2470-1173.2016.18.DPMI-007

With structures (a)–(c), variations were made only to the CFA stack section, whereas in structure (d), the silicon substrate was also modified. In recent years, several image sensor manufacturers have developed front side deep trench isolation (DTI) and backside DTI (BDTI) processes for CMOS image sensors in order to attenuate electrical crosstalk, blooming, and optical crosstalk [9], [10], [11]. The advantage of these structures in reduction of optical crosstalk in normal incidence conditions has been proven. This work aims to study the effect of BDTI on attenuation of optical crosstalk when light rays arrive at the image plane with high angles of incidence corresponding to representative steep light incidence conditions in real camera modules.

Spectral Characterization

Quantum efficiency of the four image sensors was measured in a central region-of-interest, where each part was in a package that included an IRCF with transmission spectrum that is representative for mobile imaging applications. Measurements were done when the sensor was rotated to achieve four angular positions relative to the optical axis: 0^0, 15^0, 30^0, and 45^0. QE curves of each image sensor were normalized to the maximal average green channel response in normal incidence. Error! Reference source not found. presents the 16 relative-QE curves.

Comparison of the normal incidence response shows the advantage of structure (a), RYYB, in collection of light. The yellow color filter allows a broader band of light to reach the photodiode than a green one. This allows substantial enhancement in captured signals in dim light conditions, but requires an advanced image signal processor (ISP) to maintain high fidelity of a scene's luminance and color information with low level of chroma noise, such as the ON Semiconductor (Aptina) Clarity+ technology.

With all structures, pixel responsivity decreases with increase in incidence angle. Because of the high transparency of the yellow filter, optical crosstalk is higher in structure (a), RYYB, than in structure (b), RGGB, at all angles. At 45^0, QE curves of all pixels in structure (a) are becoming highly overlapping due to the high optical crosstalk. Use of metal grid helps in preserving the shapes of the QE curves with increase in incidence angle. Best results, i.e., lowest levels of optical crosstalk with increase in incidence angle, are achieved with structure (d) that combines RGGB CFA with composite grid and BDTI. Response ratios of the different color pixels in structure (d) are maintained fairly well even at 45^0.

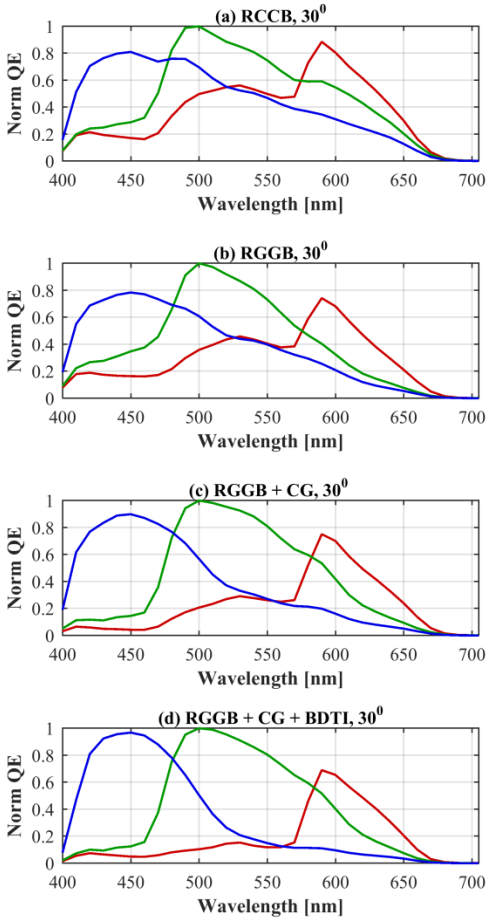

Figure 7 – Quantum efficiency curves as measured when the sensor was horizontall rotated along the optical axis by 0^0, 15^0, 30^0, and 45^0 angles. The structure that includes both composite grid and BDTI has the lowest levels of optical crosstalk at high incidence angles.

Color Properties of Synthetic Images

Synthetic raw images were prepared for all QE curves from **Figure 8** according to the procedure described previously in the "Proposed Method" section. The raw images were then processed through the pipeline that is described in the same section. As measurements were done with IRCF, QE curves were only multiplied by transmission curves of a lens for mobile imaging applications (Largan 9611A1) in order to generate raw images. The illuminant that was used for simulations is a CIE-F2, whose spectrum represents a standard cool white fluorescent (CWF) light source.

Each patch in **Figure 8** includes the reference white and black regions in two of its corners. Ideally, i.e., if there is no change in optical crosstalk with increase in incidence angle, all images should be gray.

DOI: 10.2352/ISSN.2470-1173.2016.18.DPMI-007

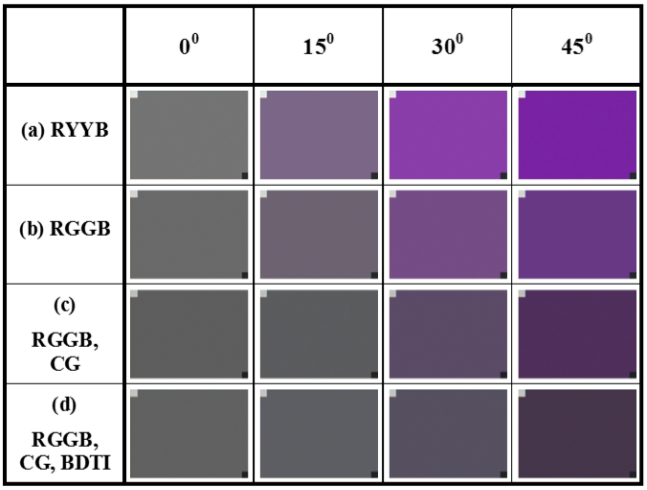

*Figure 8 – Synthetic images that were generated from the 16 quantum efficiency curves from **Error! Reference source not found.**. High change in chroma indicates that the sensor is more susceptible to chromatic flare artifacts. Subjective evaluation shows that best results are achieved with combination of CG and BDTI.*

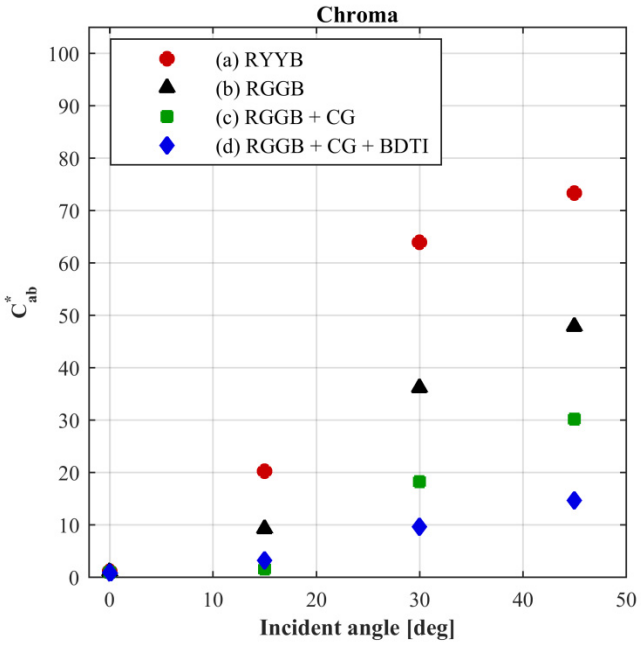

Figure 9 – Chroma of the synthetic images from Figure 8. Low change in chroma with increase in incidence angle indicates low optical crosstalk due to light rays that arrive at the image plane at high angles and, therefore, low susceptibility to chromatic flare artifacts.

Subjective evaluation of the synthetic images indicates that structure (a) exhibits the highest change in chroma with incidence angle and structure (d), whose patch color may still be considered as "gray" at 30^0 incidence angle, exhibits the lowest change in chroma. A CIE-D65 illuminant should be used to simulate outdoor flare conditions.

Figure 10 –Office images that were capture with three image sensors: (1) RGGB CFA, (2) RGGB CFA and CG, and (3) RGGB CFA with CG and BDTI. All sensors were accommodated in exactly the same module. Appearance of purple is obvious in (1), weaker in (2), and barely noticeable in (3).

Color properties were evaluated for the central region of all patches in **Figure 8**, i.e., excluding the black and white corners. **Figure 9** presents chroma values. Quantitative results confirm that structure (d) has the lowest increase in chroma for light that arrives at high incidence angle and, therefore, is the least susceptible to

DOI: 10.2352/ISSN.2470-1173.2016.18.DPMI-007

chromatic flare artifacts. Structure (c) comes in second place, and structure (a) comes last.

Figure 10 shows a set of images that were captured under fluorescent illumination using image sensors with structures (b), (c), and (d). The same camera module was used to accommodate all image sensors, and all images were processed through a conventional pipeline. One easily observes the appearance of purple in the region that surrounds the light bulbs in image (1), RGGB, a weaker artifact in image (2), RGGB and CG, and, barely noticeable purple artifact in image (3), RGGB with CG and BDTI. Therefore, there is a good agreement between the quantitative prediction of the sensor-based method and end-user image quality.

Conclusion

This work presented a method for quantifying the susceptibility of a color image sensor to chromatic flare artifacts. Experimental results quantify, for the first time, the benefits of metal-based isolation grid and BDTI in attenuation of chromatic flare artifacts. Furthermore, quantitative results exhibit good correlation with end-user image quality. Utilization of metal-based grid and BDTI in combination with yellow or clear pixels is a promising approach to exploit high pixel sensitivity that is enabled by the high transparency of the filter while minimizing chromatic flare artifacts caused by optical crosstalk.

Acknowledgment

The authors would like to thank Igor Karasev, Ning Li, Brian Keelan, Kishore Penmetsa, Jon Stern, and the CFA Technology team for their technical assistance, valuable comments and input.

Works Cited

[1] X. Chen, "Mobile phone camera lens design with reduced flare," in *Proc. SPIE 7652, International Optical Design Conference*, 2010.

[2] Imatest, "Veiling Glare AKA lens flare," [Online]. Available: http://www.imatest.com/docs/veilingglare/. [Accessed 13 01 2016].

[3] Image Engineering, "Quantifying the contrast loss caused by stray light," [Online]. Available: http://www.image-engineering.de/news/product-news/846-quantifying-the-contrast-loss-caused-by-stray-light?highlight=WyJ2ZWlsaW5nIiwidmVpbCJd. [Accessed 13 01 2016].

[4] K. Parulski and K. Spaulding, "Color image processing for digital cameras," in *Digital Color Imaging Handbook*, G. Sharma, Ed., Boca Raton, FL: CRC Press LLC, 2003, pp. 727-757.

[5] J. R. Janesick, Scientific charge-coupled devices, Bellingham, WA: SPIE - The International Society for Optical Engineering, 2001.

[6] R. S. Berns, Billmeyer and Saltzman's Principles of Color Technology, Third ed., New York, NY: John Wiley & Sons, 2000.

[7] S. Westland, C. Ripamonti and V. Cheung, Computational Colour Science Using MATLAB, 2nd ed., Chichester, West Sussex: John Wiley & Sons, 2012.

[8] R. Fontaine, "The State-of-the-Art of Mainstream CMOS Image Sensors," in *International Image Sensors Workshop*, Vaals, the Netherlands, 2015.

[9] A. Tournier, F. Leverd, L. Favennec, C. Perrot, L. Pinzelli, M. Gatefait, N. Cherault, D. Jeanjean, J.-P. Carrere, F. Hirigoyen, L. Grant and F. Roy, "Pixel-to-Pixel isolation by Deep Trench technology: Application to CMOS Image Sensor," in *International Image Sensor Workshop (IISW)*, Hokkaido, Japan, 2011.

[10] Y. Kitamura, H. Aikawa, K. Kakehi, T. Yousyou, K. Eda, T. Minami, S. Uya, Y. Takegawa, H. Yamashita, Y. Kohyama and T. Asami, "Suppression of Crosstalk by Using Backside Deep Trench Isolation," in *International Electron Devices Meeting (IEDM)*, San Francisco, USA, 2012.

[11] J. Ahn, K. Lee, Y. Kim, H. Jeong, B. Kim, H. Kim, J. Park, T. Jung, P. Wonje, T. Lee, E. Park, S. Choi, G. Choi, H. Park, Y. Choi, S. Lee, Y. Kim, Y. J. Jung, D. Park, S. Nah, Y. Oh, M. Kim, Y. Lee, Y. Chung, I. Hisanori, J. Im, D.-K. Lee, B. Yim, G. Lee, H. Kown, S. Choi, J. Lee, D. Jang, Y. Kim, T. C. Kim, G. Hiroshige, C.-Y. Choi, D. Lee and G. Han, "A 1/4-inch 8Mpixel CMOS Image Sensor with 3D," in *IEEE International Solid-State Circuits Conference (ISSCC)*, San Francisco, USA, 2014.

Author Biography

Orit Skorka received her BSc from Ben-Gurion University of the Negev, Israel, in 2001, her MSc from the Technion IIT, Israel, in 2004, and her PhD from the University of Alberta, Canada, in 2011, all in Electrical and Computer Engineering. She joined Aptina in 2013 and is now with the Image Sensor Group at ON Semiconductor. She is working on pixel characterization and image quality of CMOS image sensors for mobile imaging and automotive applications.

David Jasinski received his BS in Image Science from the Rochester Institute of Technology in 1980 and his MS in Optical Engineering from the University of Rochester in 1983. He joined Aptina in 2013 as an Imaging Algorithm Design Engineer. He is currently with the Image Processing Products Group at ON Semiconductor working on developing characterization methods and image processing techniques in support of novel image sensor designs.

Radu Ispasoiu is a senior manager of pixel R&D and image quality at ON-Semiconductor ISG (since 2014). He has held engineering management and lead R&D positions in the Silicon Valley optoelectronics technology industry for more than 15 years. He holds a PhD in Physics (1996) with focus on semiconductor optoelectronic device study from the University of Oxford, UK.

Vladi Korobov is a senior director of advanced technology development in the Image Sensor Group at ON-Semiconductor. He has held variety of senior management positions in the semiconductor field. Vladi was involved in CMOS image sensors technology for more than 18 years. He holds a PhD in EE from Tel-Aviv University, Israel.